

## RESEARCH ARTICLE

10.1002/2015JD023710

## Key Points:

- A variational scheme for analysis of high-resolution hourly rainfall
- Analysis captures the spatial pattern agreements in relatively data-sparse regions
- Analysis can particularly be beneficial and subsequent investigation of heavy rainfall events

## Correspondence to:

Y. Hong,  
yanghong@ou.edu

## Citation:

Li, H., Y. Hong, P. Xie, J. Gao, Z. Niu, P. Kirstetter, and B. Yong (2015), Variational merged of hourly gauge-satellite precipitation in China: Preliminary results, *J. Geophys. Res. Atmos.*, 120, 9897–9915, doi:10.1002/2015JD023710.

Received 1 JUN 2015

Accepted 21 AUG 2015

Accepted article online 25 AUG 2015

Published online 5 OCT 2015

## Variational merged of hourly gauge-satellite precipitation in China: Preliminary results

Huan Li<sup>1,2</sup>, Yang Hong<sup>2,3</sup>, Pingping Xie<sup>4</sup>, Jidong Gao<sup>5</sup>, Zheng Niu<sup>6</sup>, Pierre Kirstetter<sup>2,5</sup>, and Bin Yong<sup>7</sup>

<sup>1</sup>State Key Laboratory of Resources and Environmental Information System, Institute of Geographic Sciences and Natural Resources Research, Chinese Academy of Sciences, Beijing, China, <sup>2</sup>School of Civil Engineering and Environmental Sciences, University of Oklahoma, Norman, Oklahoma, USA, <sup>3</sup>Department of Hydraulic Engineering, Tsinghua University, Beijing, China, <sup>4</sup>NOAA Climate Prediction Center, Camp Springs, Maryland, USA, <sup>5</sup>NOAA/National Severe Storm Laboratory, Norman, Oklahoma, USA, <sup>6</sup>The State Key Laboratory of Remote Sensing Science, Institute of Remote Sensing and Digital Earth, Chinese Academy of Sciences, Beijing, China, <sup>7</sup>State Key Laboratory of Hydrology-Water Resources and Hydraulic Engineering, Hohai University, Nanjing, China

**Abstract** The article describes a variational scheme for the analysis of high-resolution hourly precipitation from China Meteorological Administration gauges and NOAA CMORPH satellite products in China and tests their impact on data-sparse regions and the heavy rainfall occurrences during the summer season (June–August 2009). In the variational scheme, a cost function is defined to measure the distance between analyzed precipitation field and observed rainfall quantity. A recursive filter is incorporated into the cost function which helps spread the observations to nearby grid points. Then a quasi-Newton method is used to solve the optimal estimation problem by minimizing the cost function. The adjoint technique is used to derive the gradient of cost function with respect to analysis precipitation. A series of experiments are performed to intercompare the variational analysis with the original CMORPH satellite products (CMP) and the bias-adjusted satellite products (Adj-CMP) against the observations. The best overall performance is from the variational analysis especially rainfall intensity by more than  $10 \text{ mm h}^{-1}$  with a prevailing mean relative spatial bias nearly reduction zero, and the correlation coefficient is almost around 0.5 in convection active areas. Ground cross-validation experiments in which each affected station is withdrawn at once indicated that the variational analysis can particularly be beneficial and subsequent investigation of heavy rainfall events. It also reveals that the precipitation analysis field has the ability to improve the accuracy of rainfall estimation and capture the spatial precipitation pattern agreements in relatively data-sparse regions.

## 1. Introduction

Despite its critical importance in a wide range of scientific and societal applications, accurate documentation of precipitation at a high temporal/spatial resolution remains a challenging task. Sources of information on the spatial pattern and time variations of precipitation include gauge measurements, weather radar observations, estimates derived from satellite observations in the infrared (IR) and microwave channels, and simulations/forecasts made by state-of-the-art numerical models. Gauge measurements represent precipitation at the instrument sites with a high quantitative accuracy. However, their spatial coverage is largely concentrated over populated land areas and their spatial representativeness is restricted by the spatial variations of precipitation associated with the scales of the precipitating cloud systems and the influence of underlying surface. Gridded fields of precipitation are often defined by interpolating irregularly distributed station data [e.g., Rudolf, 1993; Schneider, 1993; New et al., 2000; Beck et al., 2005; Xie et al., 2007]. Quality of these gauge-based analyses is a function of both the density and configuration of the local gauge network density [Morrissey et al., 1995; Chen et al., 2008; Xie and Xiong, 2011].

Observations of weather radars provide reasonable spatial coverage of precipitation over a region of up to ~300 km from the radar sites. Quantitative precipitation estimates from radar observations, however, suffer from multiple shortcomings including beam blockage by mountains and high buildings, beam height changes, and uncertainties in the Z-R relationship used to derive precipitation rates from the intensity of radar reflectivity [Krajewski et al., 2005; Krajewski et al., 2007; Vasiloff et al., 2007]. Similar to the gauge network discussed above, operational weather radar network is also restricted to areas with power supply. Substantial progress has been made in the past 30 years to estimate precipitation over the globe from satellite

observations in the infrared (IR) and passive microwave (PMW) channels as well as from spaceborne active precipitation radar [e.g., Arkin, 1979; Kummerow *et al.*, 1996; Ferraro, 1997; Kummerow *et al.*, 2001]. Recent efforts to integrate information from the PMW precipitation retrievals aboard low Earth orbit satellites and IR observations from geostationary platforms have led to the development and operational production of several sets of high-resolution satellite precipitation estimates. These include the Precipitation Estimation from Remotely Sensed Information using Artificial Neural Network (PERSIANN) of Hsu *et al.* [1997] and Hong *et al.* [2004], the Tropical Rainfall Measuring Mission (TRMM) Multi-sensor Precipitation Analysis (TMPA) of Huffman *et al.* [2007], the Naval Research Laboratory blended precipitation estimates of Turk *et al.* [2004], the Climate Prediction Center (CPC) Morphing technique (CMORPH) of Joyce *et al.* [2004] and Joyce and Xie [2011], and the Global Satellite Mapping of Precipitation of Ushio *et al.* [2009]. These high-resolution satellite estimates have proven to be capable of capturing the time/space variations of precipitation, especially over tropical and subtropical areas and during warm seasons, with seasonally changing and regionally varying bias and relatively largely random error [Ebert *et al.*, 2007; Hong *et al.*, 2007b; Tian *et al.*, 2007; Xie *et al.*, 2007; Shen *et al.*, 2009]. These satellite precipitation products exhibit intensity-dependent bias, overestimating (underestimating) weak (strong) precipitation. In particular, tendency for satellite-based products to underestimate the strong precipitation would greatly compromise their direct applications in the detection and quantification of extreme weather events [Tian *et al.*, 2009; Clarke, 2010].

Another source of precipitation information is the precipitation fields generated by state-of-the-art numerical weather and climate models. Especially, the new generation high-resolution global reanalyses, including the European Centre for Medium-Range Weather Forecasts Reanalysis-Interim (ERA-I) [Dee, 2011], the National Centers for Environmental Prediction Climate Forecast System Reanalysis [Saha *et al.*, 2010], and the NASA Modern-Era Retrospective Analysis for Research and Applications [Rienecker *et al.*, 2011], exhibit substantially improved performance in depicting global precipitation various upon their respective predecessors [Wang *et al.*, 2011]. Their capability in capturing cloud and precipitation variations of smaller time/space scales, however, remains an area for further improvements [Yoo *et al.*, 2011].

An effective way to improve precipitation analysis is to combine the information from individual sources of information with different error characteristics [Krajewski, 1987]. Over the recent two decades or so, several algorithms have been developed by both the hydrologists and the meteorologists to optimize the information from the gauge measurements, radar observations, and satellite observations [Xie and Hong, 2011]. While details differ in the statistical tools utilized, largely, these algorithms are designed to perform two functions, i.e., to remove biases in the radar/satellite precipitation estimates through comparisons/calibrations against gauge observations and, in some cases, also further to combine the bias-corrected radar/satellite estimates with gauge data to reduce the random error [Xie and Xiong, 2011]. Depending on the assumptions for the statistical structure of the target radar/satellite precipitation estimation biases, methods to correct bias range from applying a locally computed adjusting factor [e.g., Huffman *et al.*, 1995], interpolating local biases [e.g., Xie and Arkin, 1996], to matching the probability density function (PDF) of the target radar/satellite data against that for the co-located gauge data [e.g., Xie and Xiong, 2011]. Techniques to blend the bias-corrected radar/satellite estimates with gauge data include, among other methods, the maximum likelihood estimation [Huffman *et al.*, 1995; Xie and Arkin, 1996] and the optimal interpolation (OI) [Seo, 1999; Xie and Xiong, 2011]. Examination and cross-validation tests have demonstrated the effectiveness of these techniques in constructing precipitation analyses with improved quality compared to the individual input fields.

Successful applications of these objective analysis techniques have yielded operational production of several gauge-radar and gauge-satellite merged precipitation analyses at regional and global domains. Examples of gauge-radar merged precipitation products include the Stage IV radar precipitation analysis over Contiguous United States produced at NOAA/NCE [Lin and Mitchell, 2005], the radar-AMeDAS composite precipitation estimation product over Japan generated by the Japan Meteorological Agency [Makihara, 2000], and the National Mosaic Quantitative Precipitation Estimation high-resolution (1 km/5 min) gauge-radar merged precipitation analysis developed by NOAA National Severe Storm Laboratory [Zhang *et al.*, 2011]. Widely used operational products of gauge-satellite merged analyses or gauge-calibrated satellite precipitation estimates, meanwhile, include the Global Precipitation Climatology Project merged analyses of monthly, pentad, and daily precipitations [Huffman *et al.*, 1997; Adler, 2003; Xie *et al.*, 2003; Huffman *et al.*, 1997]; the CPC Merged Analyses of Precipitation [Xie and Arkin, 1996, 1997]; and the TRMM Multi-sensor Precipitation Analysis (TMPA) [Huffman *et al.*, 2007].

Precipitation over China exhibits substantial variations of an assortment of time and space scales. Accurate documentation of precipitation over China requires generous integration of information from various individual sources. Great progress has been made in the recent 10 years or so to design and implement automated weather stations over many Chinese provinces. As a result, reports of hourly precipitation from over 30,000 manned and automatic stations are being collected on a quasi real-time basis. Gauge-based analyses of hourly precipitation are constructed on a  $0.1^\circ$  latitude/longitude grid over Mainland of China through interpolation of quality-controlled station reports. Density of the Chinese gauge stations, however, is highly uneven, with much fewer stations installed over the western half of the country. Quality of the gauge-based analyses is therefore greatly compromised over the region. Even over the eastern half of the country where the network is quite dense, the network density is still insufficient to accurately capture the location and intensity of the maximum precipitation caused by the rapid evolution of severe storms.

As described above, blending information from gauge measurements, radar observations, and satellite estimates has proven to be an effective way to produce high-resolution, high-accuracy precipitation analyses for improved monitoring and quantitative applications. High-resolution satellite precipitation estimates, such as those produced by the Precipitation Estimation from Remotely Sensed Information using Artificial Neural Network (PERSIANN) [Hsu et al., 1997; Hong et al., 2007a], the TRMM Multi-sensor Precipitation Analysis (TMPA) [Huffman et al., 2007], and the CPC Morphing technique (CMORPH) [Joyce et al., 2004; Joyce and Xie, 2011], have been generated operationally with complete spatial coverage over China. A dense network of advanced weather radars have been installed over eastern China in recent years as part of the modernization efforts by the China Meteorological Administration (CMA). Composite maps of radar-based precipitation estimates, however, are still under development as of 2013.

The objective of this work is to develop a new technique to blend the precipitation information from multiple sources for the construction of a high-quality hourly precipitation analysis on a fine spatial resolution of  $0.1^\circ$  latitude/longitude over China. While earlier efforts to combine gauge, radar, and satellite precipitation estimates are mostly based on the optimal interpolation (OI) techniques [e.g., Seo et al., 2000; Xie and Xiong, 2011], a different approach is adopted in this work to integrate the precipitation information through a two-dimensional variational analysis (2D-VAR) framework. The prototype algorithm described in this paper aims to combine information of two types of inputs, i.e., the gauge measurements and the satellite estimates. Attention is paid in the design and development of the system to ensure that this new technique is capable of integrating precipitation information from additional sources including radar observations with slight modifications in the implementation. This paper is organized as follows: The variational scheme is presented in section 2. A brief description of sources of inputs and implementation of the algorithm are provided in section 3. Section 4 discusses the merged product into the improvement of the spatial extent of the accurate precipitation and details the variational analysis (var-anal) applied to the two heavy precipitation events during the summer season (June–August 2009), while conclusions are presented in the final section.

## 2. Variational Scheme

Optimal interpolation (OI) and variational scheme are two widely used objective techniques in constructing atmospheric and oceanic analyses. First proposed by Gandin [1965], the OI technique defines analyzed geophysical fields by modifying the first guess using available observations. Optimal analysis is computed for each grid point and for each time step through minimizing the expected error variance. Accurate definition of the error structure for both the first guess and the observations is a prerequisite for the success of an OI-based objective analysis [Lorenz, 1981]. The variation approach [e.g., Derb, 1987], meanwhile, defines the analysis by optimizing the overall performance of the analysis over the entire target time-space domain expressed as a cost function. One big advantage of the variational approach is the flexibility to include constraints as part of the cost function, facilitating the explicit consideration of physical consistency and time/space continuity of the geophysical fields [e.g., Japan Meteorological Agency, 1990]. In addition, error definition for the first guess and observations is simplified under the variational framework. This avoids uncertainties introduced by assumptions for the error structure for regions with poor observations [Kalnay, 2003]. Both the OI and the variational techniques have been successfully applied to construct observation-based gridded analyses of sea surface temperature [Reynolds and Smith, 1994; Thiébaux et al., 2003;

Wang and Xie, 2006], precipitation [Xie and Xiong, 2011], and other geophysical variables [e.g., Xie et al., 2012], through synthesizing information acquired from in situ measurements and satellite observations.

In this work, we aim to develop a variational-based technique to construct a two-dimensional, high-resolution precipitation analysis through integrating information from gauge observations and satellite estimates. The concept of a variational method is to determine the analysis by direct minimization of a cost function. Here the cost function is written as

$$J(p) = \gamma_G [H(F(p)) - G_O] O_G^{-1} [H(F(p)) - G_O]^T + \gamma_S [H(F(p)) - S_O] O_S^{-1} [H(F(p)) - S_O]^T \quad (1)$$

where  $p$  is the control variable (precipitation) or the target analysis variable (precipitation) at regular grid points,  $S_O$  represents the satellite observations,  $G_O$  is the gauge observation,  $F$  represents a recursive filter which helps to spread the impact of observations to nearby grid points,  $H$  is a bilinear interpolation operator that interpolates analysis variables to observation locations, and  $\gamma_G$  and  $\gamma_S$  are the weighting factors for the gauge observations and the satellite observations, respectively. They are selected to account for the relative accuracies of the two input fields, determining their relative strength of their constraints to the final analysis. The two terms measure the departure of the analysis  $H(F(p))$ , from the gauge observation  $G_O$  and satellite observations  $S_O$ , and are weighted by the inverse of the observational error covariance matrix  $O_G^{-1}$  and satellite covariance matrix  $O_S^{-1}$ , respectively. Their optimal values are determined by statistic error of each type of observation. These values can be determined through numerical experiments in a trial-and-error fashion too [Sun and Crook, 2001]. The aim of a variational scheme is to find the state of  $p$  for which the best least squares fit between the analysis field and the original observations with an iterative minimization of a cost function  $J$ .

At the minimum, the derivative of the gradient of the cost function  $J$  with respect to control variable  $p$  vanishes and the optimal estimate of  $p$  satisfies

$$\frac{J(p)}{\partial p} = \gamma_G F^T H^T O_G^{-1} [H(Fp) - G_O]^T + \gamma_S F^T H^T O_S^{-1} [H(Fp) - S_O]^T = 0 \quad (2)$$

where  $F^T$  is the adjoint of recursive filter operator and  $H^T$  is the adjoint of the bilinear interpolation operator  $H$ . The role of  $H^T$  is equivalent to bring the impact of each observation from the observational space back to the analysis grids. The adjoint operators  $F^T$  and  $H^T$  can be derived and coded using the method described in Errico [1997]. The recursive filter  $F$  is implemented by sequentially applying the following equation (3) to the analysis variable  $p$  in two-dimensional directions when calculating the cost function (1). This filter is an effective means for spreading the influence of each observation to nearby grid points, thus ensuring a reasonably smooth analysis. Following the work of Purser and McQuigg [1982], Lorenc [1992], and Hayden and Purser [1995], a one-dimensional recursive filter is given by

$$Y_i = \alpha Y_{i-1} + (1 - \alpha) X_i \quad \text{for } i = 1, \dots, n \\ Z_i = \alpha Z_{i+1} + (1 - \alpha) Y_i \quad \text{for } i = n, \dots, 1 \quad (3)$$

where  $X_i$  is the initial value at grid point  $i$ ,  $Y_i$  is the value after filtering for  $i = 1$  to  $n$ ,  $Z_i$  is the initial value after one pass of the filter in each direction, and  $\alpha$  is the filter coefficient given by the following formulation [Lorenc, 1992]:

$$\alpha = 1 + E + \sqrt{E(E + 2)} \\ E = N \Delta x^2 / L^2 \quad (4)$$

where  $L$  is the horizontal correlation scale,  $\Delta x$  is the grid spacing, and  $N$  is the number of filter passes to be applied. Equation (4) is a first-order recursive filter, applied in both directions to ensure zero phase change. Multipass filters ( $N > 1$ ) are developed by repeated applications of equation (4). A two-dimensional filter was constructed by applying this one-dimensional filter successively in each coordinate direction. It can be shown that such multidimensional filters, when applied with several passes, can accurately model error correlations [Purser et al., 2003; Gao et al., 2004]. A first-order recursive filter is applied in both directions to make sure that the initial zero or model phase has been changed.

Given the sparse conventional observational network, the var-anal is insensibility for the first guess/background field, whereas is understandably sensitive to inputs parameterization implementation. The procedure for solving the variational problem is as follows:

1. Choose a first guess for precipitation field  $p$  (usually zero or guessed climate values).
2. Apply the two-dimension recursive filter to the guess field  $p$  and use the forward operator  $H$  to interpolate  $p$  from analysis grids to observation points.
3. Calculate the cost function  $J(p)$  according to equation (1).
4. Calculate the gradient of the cost function at each grid point (equation (2)) using the adjoint technique [e.g., Talagrand and Courtier, 1987; Courtier et al., 1998].
5. Use a quasi-Newton minimization algorithm [Liu and Nocedal, 1989] to obtain updated values of the analysis variable  $p$  at each grid point as follows:

$$p^n = p^{(n-1)} + \sigma \cdot f(\partial J/\partial p) \tag{5}$$

where  $n$  is the iteration number,  $\sigma$  is the optimal step size obtained by the “line search” process in optimal control theory [Grill et al., 1981], and  $f(\partial J/\partial p)$  is the optimal descent direction obtained by combining the gradients from several previous iterations.

Check whether the optimal solution for  $p$  has been found. This is done either by (a) computing the value of  $J(p)$  to determine if it is less than a prescribed tolerance or (b) determining if a specified maximum number of iterations have been reached. If either criterion is satisfied, then stop iterating. Otherwise, repeat steps 2 through 6 using the updated field of  $p$  as the new guess.

### 3. Data and Implementation

#### 3.1. Data

In this work, the 2D-VAR-based blending technique is developed using gauge-observed and satellite-estimated hourly precipitation data over China for the summer season period from June to August 2009. Despite the relatively short period, precipitation observed during the month is typical of that for the summer season over China, characterized by precipitation events caused by large scale as well as mesoscale weather systems. Gauge data used in this study are hourly precipitation reports from ~29,000 stations over the Mainland of China collected and quality controlled by the China Meteorological Administration (CMA) National Meteorological Information Center. Most of these stations are concentrated over the eastern half of the country, while gauge stations are much sparser over the western half (Figure 1a). CMORPH satellite precipitation estimates of Joyce et al. [2004] are used as the second piece of inputs to the 2D-VAR-based hourly precipitation analysis system. The original CMORPH precipitation data are generated at an 8 km × 8 km grid over the globe (60°S–60°N) and in a time interval of 30 min. In this study, the raw CMORPH precipitation data are integrated into a grid of 0.1° latitude/longitude and averaged into hourly accumulation (Figure 1b).

#### 3.2. Removing Satellite Bias

CMORPH presents similar patterns of hourly precipitation with those from the gauge-based analysis over China, while systematic errors exist in its overall magnitude (Figure 1c). This systematic error (bias) in the CMORPH satellite estimates must be removed before variational analysis may be applied to combine the satellite data with the gauge observations. To this end, a bias correction procedure similar to that of Boushaki et al. [2009] is adopted. First, CMORPH bias ( $E_i$ ) at a given 0.1° latitude/longitude grid box ( $i$ ) is computed for the target hourly time step as the weighted mean of gauge-CMORPH differences over 0.1° latitude/longitude grid boxes within 0.25° latitude/longitude from the target grid box:

$$E_i = \frac{\sum_{n \in \Omega_i} [\omega_n (G_n - S_n)]}{\sum_{n \in \Omega_i} \omega'_n} \tag{6}$$

where  $G_n$  and  $S_n$  are, respectively, gauge observations and CMORPH satellite estimates at a 0.1° latitude/longitude grid box ( $n$ );  $\Omega_n$  denotes the neighborhood region centered at the target grid box ( $i$ ), while  $\omega_n$  is the weighting factor accounting for the gauge density and the distance between the target grid box ( $i$ ) and the pixel ( $n$ ), defined as

$$\omega_n = \omega_{nd} \times \omega_{ng} \tag{7}$$

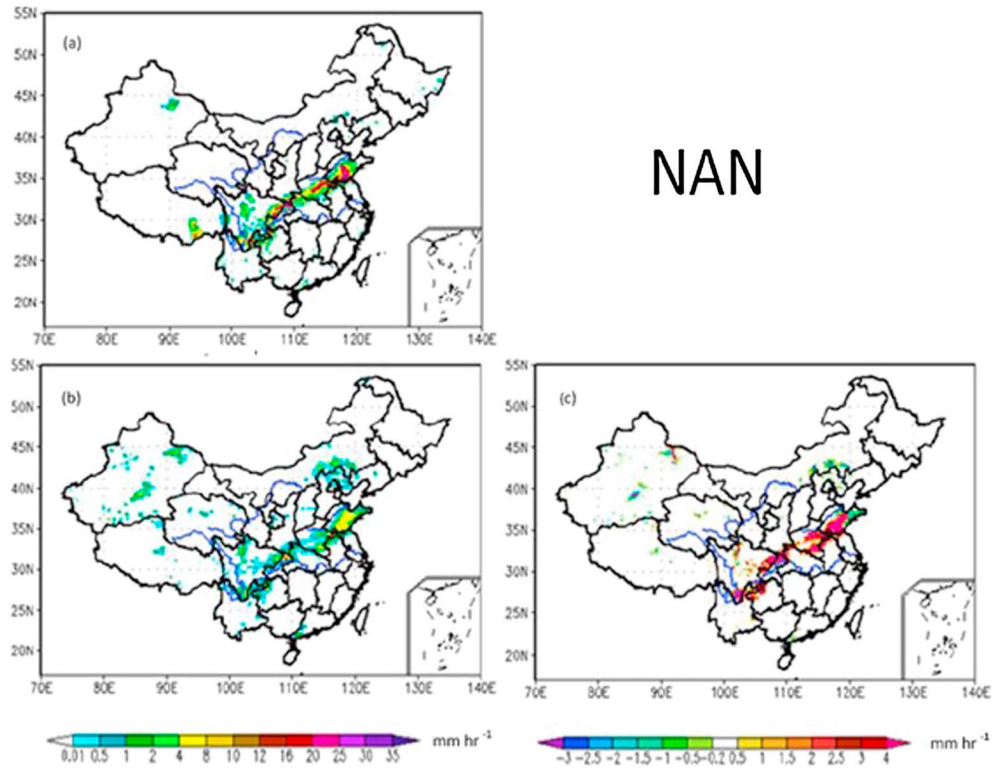


**Figure 1.** Hourly precipitation (mm/h) over the Mainland of China for 02:00 UTC, 11 July 2009, derived from (a) the grid box mean of CMA station hourly reports, (b) CMORPH satellite estimates, and (c) their differences relative to the gauge data (mm h<sup>-1</sup>).

where  $\omega_{nd}$  is the distance weighting factor while  $\omega_{ng}$  is a function accounting for the refined quantitative accuracy calculated using gauge data over a grid box with more reporting gauges:

$$\omega_{nd} = \frac{D^2 - d_n^2}{D^2 + d_n^2} \tag{8}$$

where  $d_n$  is the distance between the target grid box ( $i$ ) and the grid box ( $n$ ) where the gauge-satellite differences are computed and  $D$  is the maximum distance, set to 30 km in this study.

The gauge density weighting function varies with the number of reporting gauges inside the grid box, set to zero if the number of gauges is less than  $\epsilon$  and to a unit if the number is larger than  $\alpha$ :

$$\omega_{ng} = f(N, \epsilon, \alpha) = \begin{cases} 0 & (N < \epsilon) \\ N/\alpha & (\epsilon < N < \alpha) \\ 1 & (N > \alpha) \end{cases} \tag{9}$$

The gauge-CMORPH differences computed hourly by equation (6) presents substantial frustrations. To achieve stable statistics, the hourly differences are smoothed over a 31 day period centering at the target day and applied to define the bias-corrected CMORPH ( $P_A^i$ ) from the raw satellite estimates ( $P_S^i$ ):

$$P_A^i = P_S^i + \frac{P_S^i}{\sum_{j \in \Omega_i} P_S^j} \sum_{j \in \Omega_i} [\bar{E}_j] \tag{10}$$

where  $\Omega_i$  is the 31 day smoothing period.

### 3.3. Quantifying Error

Key to the success of a precipitation analysis is the accurate quantification of the errors for the inputs. Huffman et al. [1997] developed a sophisticated formulation to compute the error variance of satellite estimates

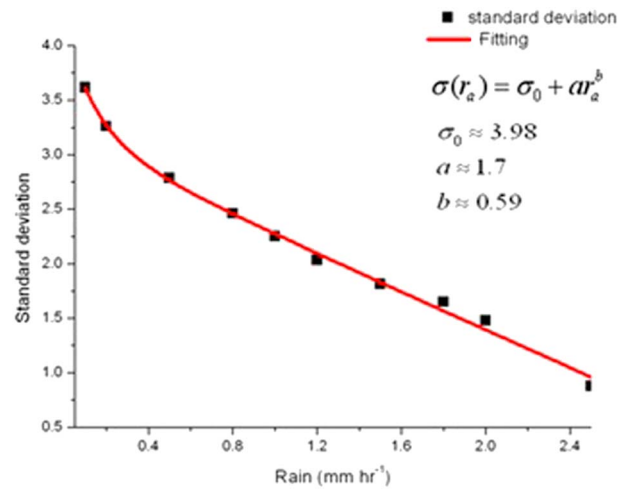


**Figure 2.** Scatterplots (black filled squares) between the standard deviation of conditional rainfall intensity and the rainfall intensity over 10 km pixels at hourly time scales and an empirical model of the standard deviation as a function of the rainfall intensity (red line) based on the least squares fitting of the scattered dots.

about gauge rainfall error and satellite precipitation error statistics, several assumptions have been made here: matrices  $O_G$  and  $O_S$  are assigned to be diagonal (i.e., no spatial correlation among gauge observations error), and  $\sigma$  has been specified for the error standard deviation of hourly accumulated precipitation amounts. The standard deviation of precipitation intensity ( $\sigma$ ) is modeled as a function of precipitation intensity ( $r_a$ ). Following the practice of Villarini et al. [2008] and [Villarini and Krajewski, 2008], a three-parameter power law function is taken:

$$\sigma(r_a) = \sigma_0 + ar_a^b \tag{11}$$

where  $\sigma$  is the standard deviation. Proportional constant is determined through comparison with gauge analysis over grid boxes with at least one gauge using data over Mainland of China for the summer season in 2009 shown in Figure 2. The coefficients  $\sigma_0$ ,  $d$ , and  $e$  are set to 3.98, 1.7, and 0.59, respectively, through the least squares fitting of rain gauge and satellite data.

### 3.4. Error Correction

The last parameter we need to specify to perform the variational analysis is the correction between errors that occurred over two separate points for the target precipitation field. We assume that the error correlation is a function of the distance between the two points, expressed as an exponential function of the negative distance for CMORPH. This is often defined by computing the  $e$ -folding distance of the spatially logged correlation for the target field [Habib and Ciach, 2001]. For gauge observations, the correlation between errors at two different locations is zero. To this end, we computed correlation between the time series of hourly precipitation at two 0.1° latitude/longitude grids with various separation distances over China. We then stratified the computed correlation as a function of the separation distance and modeled the spatial correlation as a three-parameter exponential function of the separation. As shown in Figure 3, the spatial correlation in CMORPH error declines rapidly with the distance, from ~0.9 at a distance of ~10 km to ~0.5 at ~30 km. The  $e$ -folding distance for the hourly precipitation over a 0.1° latitude/longitude grid box is computed as 23.7 km in this study. In this test, the  $e$ -folding distance is arbitrarily set to 24 km.

## 4. Results and Validation

### 4.1. Visual Comparisons

The variational scheme is developed based on the assumptions that gauge reports are unbiased with reasonable gauge network and that satellite estimates are generally biased but contain useful information on the spatial distribution patterns of precipitation. Figure 4 illustrates an example of the hourly precipitation maps over Mainland of China for 01:00 Z, 8 July 2009, generated by the gauge-based analysis (top left) [Shen et al., 2009],

of precipitation as a polynomial function of precipitation intensity and sampling size, reflecting the trend of the random error to increase with the precipitation intensity and decrease with the sampling size, respectively. Xie and Xiong [2011] simplified the formula of Huffman et al. [1997] to assume that the error variance is proportional to the precipitation intensity and inversely proportional to the sampling size and determined the coefficients using real data.

In this study, a slightly different approach is taken. Following [Lopez and Bauer, 2005] and Lopez [2010], we relate the magnitude of the error for the input precipitation fields to the local spatial variability of the target precipitation fields. Matrices  $O_G$  and  $O_S$  in equation (1) are supposed to describe observation errors and satellite estimate errors in terms of variances (diagonal terms) and covariances (off-diagonal terms). Since little is known

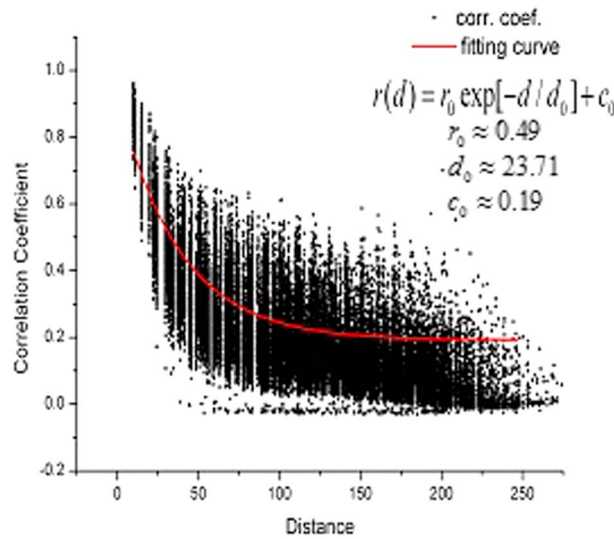


**Figure 3.** Correlation between hourly precipitation error at two locations as a function of separation distance, computed using 0.1° latitude/longitude gridded gauge analysis over China (black filled squares) and modeled as a three-parameter exponential function through the least squares fitting (red line). The e-folding distance of the spatially lagged hourly precipitation is 23.71 km in this calculation.

generate suspicious “bull’s-eye” patterns where raining areas are unrealistically spread out in interpolating rainfall reported by isolated stations. The original CMORPH satellite estimates (Figure 4b) were capable of capturing the

the original CMORPH satellite estimates (top right) [Joyce *et al.*, 2004], the bias-CMORPH through adjustment against the gauge data (bottom left), and the final blended precipitation analysis through our variational technique (bottom right). As shown in the gauge-based analysis, a major weather system was proceeding over northern China, causing a band of heavy precipitation over the region with a maximum of over 50 mm h<sup>-1</sup> in the Shangdong Provinces (Figure 4a). The gauge network density, as displayed in Figure 1, is very sparse over the Tibetan high plateau. As a result, the gauge-based analysis defined by interpolating reports from these sparsely distributed stations may have missed some small-scale precipitation systems captured by the CMORPH satellite estimates (Figure 4b). At the same time, the gauge-based analysis may also gener-

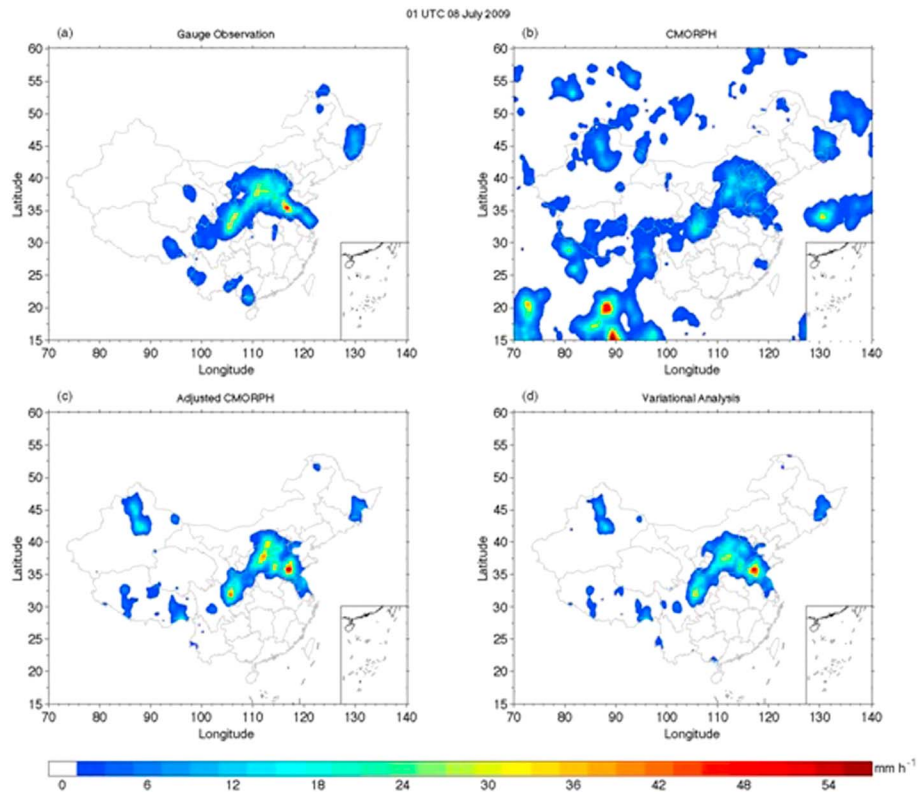


**Figure 4.** Distribution of hourly precipitation over China for 01:00 UTC, 08 July 2009, derived from (a) the gauge-based analysis, (b) the original CMORPH satellite estimates, (c) the bias-corrected CMORPH, and (d) the gauge-CMORPH blended precipitation analysis through our variational technique. Unit is mm h<sup>-1</sup>.

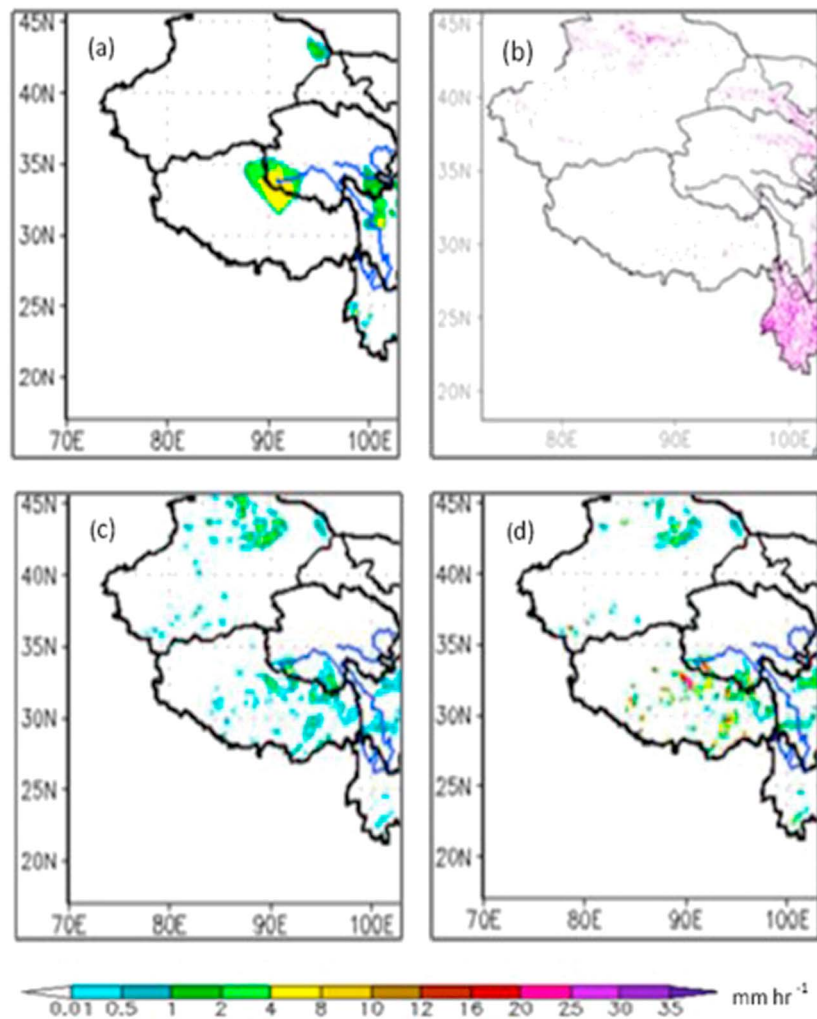


**Figure 5.** Merged analysis used in gauge sparse regions, derived from (a) gauge-based rainfall, (b) stations distribution, (c) CMORPH, and (d) gauge-CMORPH blended precipitation analysis through variational technique over Tibetan Plateau.

overall structure of the precipitation systems over the entire target domain. The magnitude of the CMORPH precipitation, however, was significantly lower for the heavy rainfall compared to the gauge data. This tendency of underestimating precipitation is attributable to the saturated response of the passive microwave observations to radiance emitted from a column of atmosphere associated with heavy rainfall events.

After the bias correction procedure developed in this study through comparison against the concurrent gauge observations, the magnitude of the bias-adjusted CMORPH (Figure 4c) is in much improved agreement with the gauge analysis, while the overall distribution patterns remain similar as those in the original CMORPH. In particular, the maxima of precipitation were much better reflected in the bias-corrected CMORPH, indicating substantial improvements in CMORPH's capability to capture severe weather events. The variational analysis succeeded in producing precipitation analysis with further improved quality, taking advantage of the strengths from both the input gauge data and the bias-corrected CMORPH satellite estimates. The overall spatial pattern of precipitation is similar to that of the CMORPH estimates, while the magnitude of the precipitation analysis is very close to the gauge analysis where the station network is dense and the gauge analysis is more reliable (e.g., over the east coast of China). Due to extrapolation of heavy rainfall at isolated stations, unrealistic distribution patterns (Figure 5a) observed over gauge sparse western China are removed/modified with the inclusion of spatial patterns from the CMORPH through the 2D-VAR procedure (Figures 5c and 5d). Precipitation field of fine spatial structure is well captured over Tibetan high plateau where gauge network is relative sparse. Qualitatively

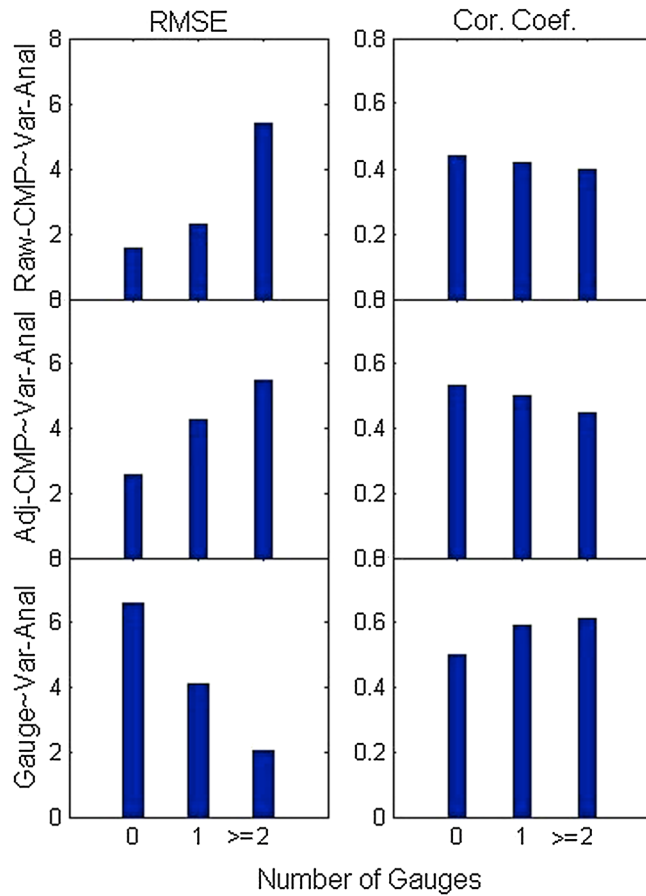


**Figure 6.** (left) Root-mean-square (RMS) (mm h<sup>-1</sup>) and (right) correction coefficient are computed through comparison of (top) original CMORPH, (middle) adjusted CMORPH, and (bottom) variational analysis against the withdrawn gauge observations of hourly precipitation over Mainland of China grid boxes with 0, 1, and 2 and more gauges.

speaking, the bias-adjusted and the 2D-VAR procedures succeeded in blending the information from the gauge observations and the satellite estimates as we designed.

**4.2. Mainland of China-Wide Direct Evaluation**

A suite of cross-validation tests was conducted to quantify the performance of the original CMORPH, bias-corrected CMORPH, and the variational analysis in representing the spatial-temporal variations of hourly precipitation over China. Special emphasis has been put to assess the above-mentioned products' capability in detecting and quantifying extreme precipitation events. To this end, reports of hourly precipitation at 10% randomly selected Chinese stations are withdrawn. Reports from the remaining 90% of the stations are used to create the gauge-based analysis, bias-adjusted CMORPH, and the variational analysis, following the procedures described in sections 2 and 3. This process is repeated for 10 times so that report at each station is withdrawn once. The original CMORPH, bias-corrected CMORPH, and the variational analysis of hourly precipitation at their raw resolution (0.1° latitude/longitude) are then

compared against the withdrawn station reports at their corresponding station locations. Only gauge data over grid boxes with at least one gauge were included in the cross validation to ensure that the variational analysis is used as the "ground truth" in reasonable quality. The comparison statistics are examined to assess the performance of the CMORPH precipitation estimates and the variational analysis.

**4.2.1. Comparison With Number of Gauges**

Comparison with different number of gauges is performed among the valid gauge observation, the original CMORPH, the adjusted CMORPH, and variational analysis to access if or not the variational process works as we designed. Figure 6 is computed root-mean-square (RMS) error, and correction coefficients among the four data sets are calculated for grid boxes with various numbers of stations and for the entire data period from 1 June to 31 August 2009. The values (differences) between the gauge and the satellite estimates (CMORPH and adjusted CMORPH) are minimum over grid boxes and increase substantially over regions with gauge station (Figure 6, top left and middle left). The differences between the variational analysis and gauge are very large over grid boxes with no gauges and decreases as local gauge network becomes dense (Figure 6, bottom left). The correction coefficient is higher when the numbers of gauges are more shown in the right plot of Figure 6. These results indicate that the variational analysis over gauge sparse regions is controlled primarily by satellite estimates while it is influenced more by gauge analysis where station reports are available, confirming that our objective algorithm works as we design.

Table 1 presents cross-validation statics for relative bias, RMS error, and correlation coefficient comparison against withdraw valid gauge for the target test period, June–August 2009. As reported in earlier studies

**Table 1.** Relative Bias (%), RMS ( $\text{mm h}^{-1}$ ) Error, and Correlation Coefficient Between Validation Data and Original CMORPH (CMP), Adjusted CMORPH (Adj-CMP), and the Gauge-CMORPH Variational Analysis (Var-Anal), Add One Column to Show the Averaged Hourly Rainfall From Valid Data for Each Month and Overall

	CMP			Adj-CMP			Var-Anal		
	Bias (%)	RMSE ( $\text{mm h}^{-1}$ )	Correlation Coefficient	Bias (%)	RMSE ( $\text{mm h}^{-1}$ )	Correlation Coefficient	Bias (%)	RMSE ( $\text{mm h}^{-1}$ )	Correlation Coefficient
June	5.9666	13.3935	0.0233	3.4913	11.9228	0.3369	1.7078	6.5143	0.5224
July	-1.151	7.7493	0.4178	0.0352	7.2302	0.5258	-0.09	6.0622	0.5933
August	4.9851	12.9311	-0.0023	2.8378	11.4844	0.2336	2.0783	7.9124	0.4019
Total	3.687	10.8409	0.1694	2.2118	9.7466	0.3741	0.7078	6.5143	0.5620

[Xie *et al.*, 2007; Shen *et al.*, 2009; Xie and Xiong, 2011], the original CMORPH satellite precipitation estimates (column 2) exhibit bias of nonnegligible magnitude that changes with both time and region. After the gauge-correction procedure is implemented, the bias in CMORPH is reduced substantially (column 8). The variational processing further lowers the bias a very small magnitude. At the same time, pattern agreement, reflected by the random error (column 9) and the correlation (column 10), is also improved consecutively through implementing the bias correction and the variational analysis procedure. Overall, as shown in Table 1, the bias has been reduced from 3.687% of the mean gauge-measured precipitation in the original CMORPH to 2.2118% in the gauge-corrected CMORPH and to 0.7078% in the final variational analysis. At the same time, the pattern correlation is improved from 0.1694 for the original CMORPH to 0.3741 for the gauge-corrected CMORPH and 0.5620 for the final variational analysis, respectively. These cross-validation statistics clearly demonstrated that the bias correction and the variational analysis algorithms developed in this study are capable of constructing gauge-satellite blended hourly precipitation analysis with overall improved quantitative accuracy upon the input data.

#### 4.2.2. Rainfall Intensity-Based Evaluation

Precipitation and its interactions with other hydrological and hydrometeorological processes are highly non-linear. It is therefore very important to assess the performance of our precipitation analyses in detecting and quantifying precipitation events of various intensities. To this end, we grouped the cross-validation test data into seven categories based on the hourly precipitation intensity and computed the comparison statistics for each of the groups. As shown in Table 2 and Figure 7, the original CMORPH satellite estimates tend to overestimate/underestimate the magnitude for weak/strong precipitation events. In particular, the original CMORPH may underestimate the intensity by more than  $10 \text{ mm h}^{-1}$  for a precipitation event of  $20 \text{ mm h}^{-1}$  or stronger. After the bias correction and the variational analysis, the bias in final gauge-satellite blended precipitation is reduced substantially for precipitation events of all intensities. At the meantime, pattern correlation for the blended precipitation analysis is also improved compared to the original CMORPH satellite estimates, although the comparison statistics is less stable restricted by the relatively small size of cases.

#### 4.3. Regional-Based Cross Validation

Summer precipitation exhibits substantial regional variations. In general, precipitation over southeastern China is more or less dominated by organized deep convections, that over northeastern is more associated with large-scale synoptic weather systems, and that over dry western inland regions is produced by clouds

**Table 2.** Cross-Validation Results for Cases of Different Precipitation Intensities

Rainfall Intensity	CMP			Adj-CMP			Var-Anal		
	Bias (%)	RMSE ( $\text{mm h}^{-1}$ )	Correlation Coefficient	Bias (%)	RMSE ( $\text{mm h}^{-1}$ )	Correlation Coefficient	Bias (%)	RMSE (%)	Correlation Coefficient
<1.0	8.7436	9.7943	0.0019	7.6721	9.6682	-0.3474	6.2959	7.3608	0.7203
1.0-2.0	8.3315	8.4371	0.0887	5.6220	7.8776	0.4410	3.0789	5.6538	0.5040
2.0-5.0	3.5589	8.2891	0.0321	2.3999	7.9032	0.1720	1.2417	5.4938	0.3524
5.0-10.0	1.4332	7.7526	0.0165	1.0122	7.5886	0.1164	0.4834	5.1872	0.1838
10.0-15.0	0.6857	6.7800	0.0728	0.5390	6.8278	0.1770	0.2630	4.8321	0.2466
15.0-20.0	0.3632	5.5235	0.0217	0.3202	5.7952	0.1209	0.1784	4.3134	0.2497
>20.0	-0.6683	8.0219	0.1484	-0.6545	7.4797	0.4671	-0.1137	4.4746	0.6282

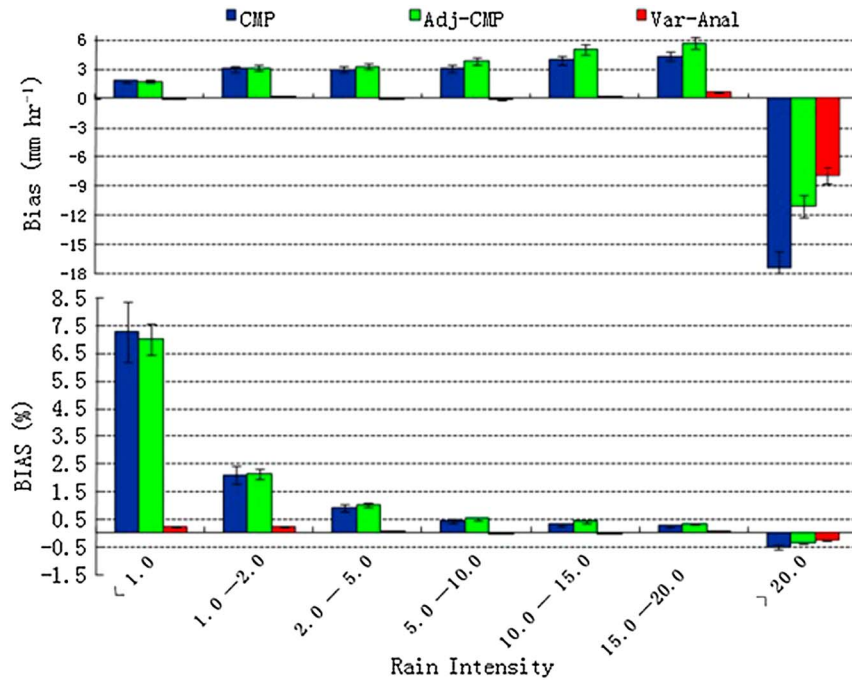


**Figure 7.** (top) The mean bias ( $\text{mm h}^{-1}$ ) and (bottom) relative bias (%) for the original CMORPH (black), bias-corrected CMORPH (green), and the variational analysis (red) derived using data from the cross-validation tests. Results are computed and presented for seven groups stratified based on the precipitation intensity from the gauge data.

with relatively shallow depth and limited atmospheric moisture. Performance of satellite-based precipitation estimates rely heavily on the type (convective/stratiform) of precipitation. It therefore will present regional variations over China. Meanwhile, gauge station network density changes greatly over China, with much denser local networks over populated well and industrialized eastern regions and very sparse networks on the western parts of the country.

To examine the relative performance of our gauge-satellite blending technique, we computed the comparison statistics for the cross-validation tests for several regions inside China. For this purpose, the entire Mainland of China is divided into eight regions, marked as regions a, b, c, d, e, f, g, and h, as shown in Figure 8. Among the eight regions, Region c covers the majority of the Yangtze-Huai River basin, while

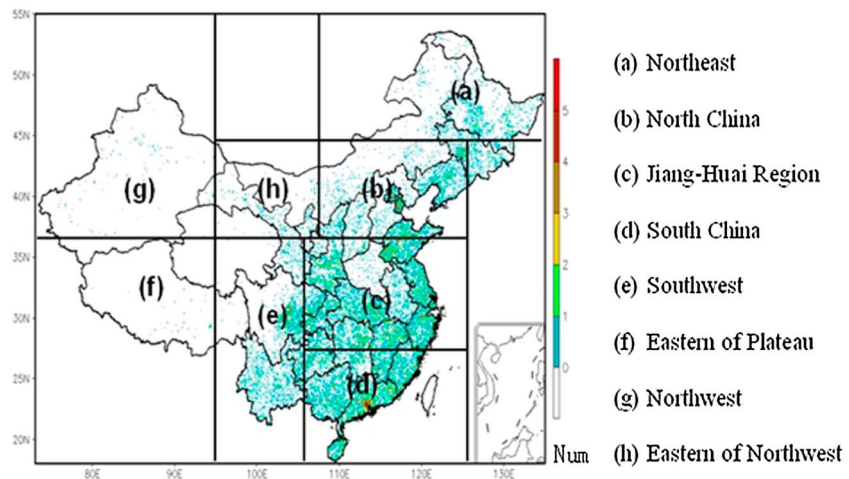


**Figure 8.** Number of station reports available in a  $0.1^\circ$  latitude-longitude grid at 04:00 UTC, 08 July 2009. The eight geographical domains are divided from the terrain and gauge density for the computations of precipitation validation: Northwest, north China, Jiang-Huai region, south China, Southwest, Eastern of Plateau, Northwest, and Eastern of Northwest.

**Table 3.** Same as in Figures 9 and 10<sup>a</sup>

	CMP			Adj-CMP			Var-Anal		
	Bias (%)	RMSE (mm h <sup>-1</sup> )	Correlation Coefficient	Bias (%)	RMSE (mm h <sup>-1</sup> )	Correlation Coefficient	Bias (%)	RMSE (mm h <sup>-1</sup> )	Correlation Coefficient
(a) Northeast	6.1197	7.1925	0.1651	3.9096	6.2350	0.1704	3.1638	4.1032	0.5682
(b) North China	5.9171	6.9569	0.2079	3.2977	5.7892	0.2398	2.8709	3.8229	0.6235
(c) Jiang-Huai region	7.2753	9.8246	0.2405	3.1238	7.7431	0.3159	3.1295	4.9480	0.7051
(d) South China	8.0825	10.1983	0.1928	5.5803	10.028	0.2231	5.0678	6.7452	0.5892
(e) Southwest	5.4800	9.206	0.1940	3.0429	8.3244	0.2333	1.0198	5.6100	0.5956
(f) Eastern of Plateau	7.9452	5.9840	0.1150	4.6180	4.8686	0.1199	3.7117	3.1529	0.5048
(g) Northwest	6.7946	4.8928	0.1079	4.0614	4.1555	0.0978	3.3961	2.9447	0.4734
(h) Eastern part of Northwest	6.4738	4.9486	0.1661	2.4128	3.1085	0.1826	2.2403	2.0608	0.6060

<sup>a</sup>Cross-validation statistics for the original and gauge-adjusted CMORPH and analysis of hourly precipitation against the validated data in eight divided regions over China.

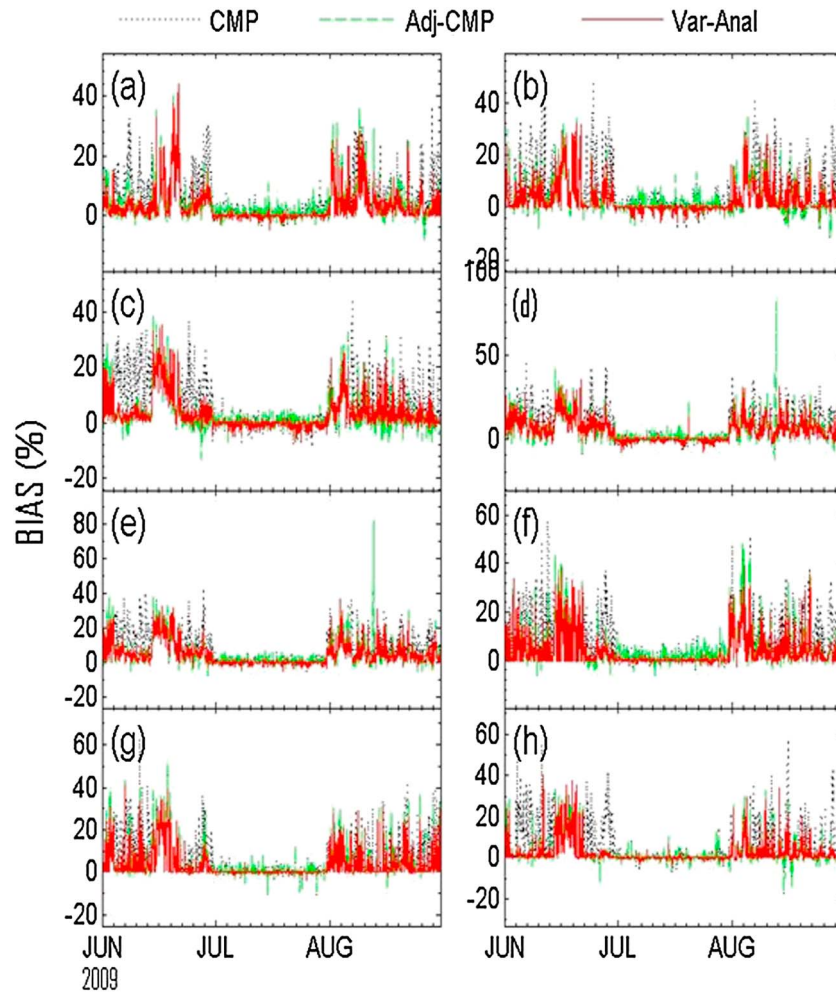


**Figure 9.** Cross-validation statistics for the original and bias-adjusted CMORPH data and variational analysis of hourly precipitations in (a) Northwest (42.5–55°N, 110–135°E), (b) north China (35–42.5°N, 110–125°E), (c) Jiang-Huai region (27.5–35°N, 107.5–125°E), (d) south China (15–27.5°N, 107.5–125°E), (e) Southwest (22–35°N, 97.5–107.5°E), (f) Eastern of Plateau (27.5–35°N, 126–200°E), (g) Northwest (35–50°N, 72–97.5°E), and (h) Eastern of Northwest (35–42.5°N, 97.5–110°E). Bias values appear in Table 3.

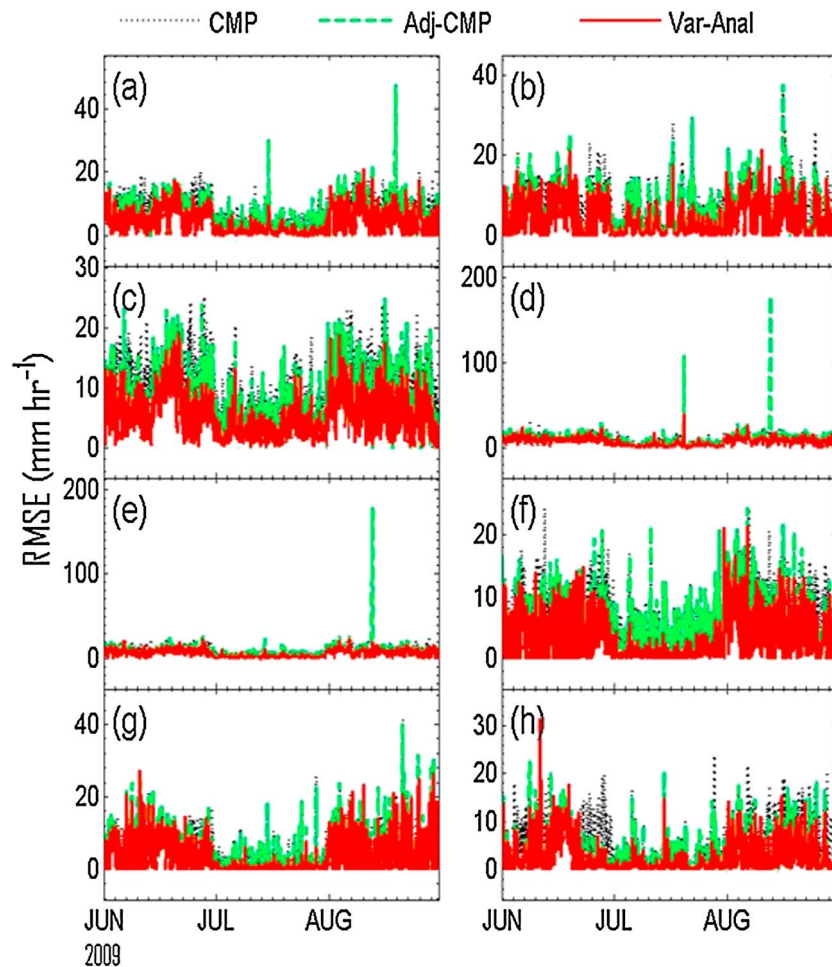


**Figure 10.** Same as Figure 9 but for RMSE, which values are detailed in Table 3.

Region d is located over southern China; precipitation over both regions are dominated by convective heavy rainfall over the target period of this study. Regions f and g, meanwhile, are Tibetan high plateau and the semiarid northwestern China, respectively, with precipitation from scattered cloud systems during our study period.

Despite the differences in both the precipitation systems and the observing gauge networks and satellite estimates, the gauge-satellite blending technique developed in this study is capable of reducing the bias in the original CMORPH satellite estimates and improving the pattern correlations for the precipitation analysis (see Table 3 and Figures 9 and 10 for details). For example, over the southwest China (Region g), the bias and correlation are 5.48% and 0.1940, respectively, for the original CMORPH, improved to 1.0198% and 0.5956 for the variational analysis. In general, the final gauge-satellite blended analysis (after the variational processing) exhibits slightly superior performance, especially in pattern correlation, over eastern China that over the western regions. This performance difference is likely attributable to the combination of better performance of the original satellite precipitation estimates and the denser gauge network over western China.

**4.4. Application**

In order to test the potential utility of the variational analysis for hydrological applications, the temporal distributions of precipitation-averaged rain rates are displayed from each of the five respective areas (over specific basins such as the Yangtze River basin, the heavy rainfall occurrence at the south China region, and southwest of Jiangsu Province, and the data-sparse region Tibetan Plateau) shown in Figure 11. The

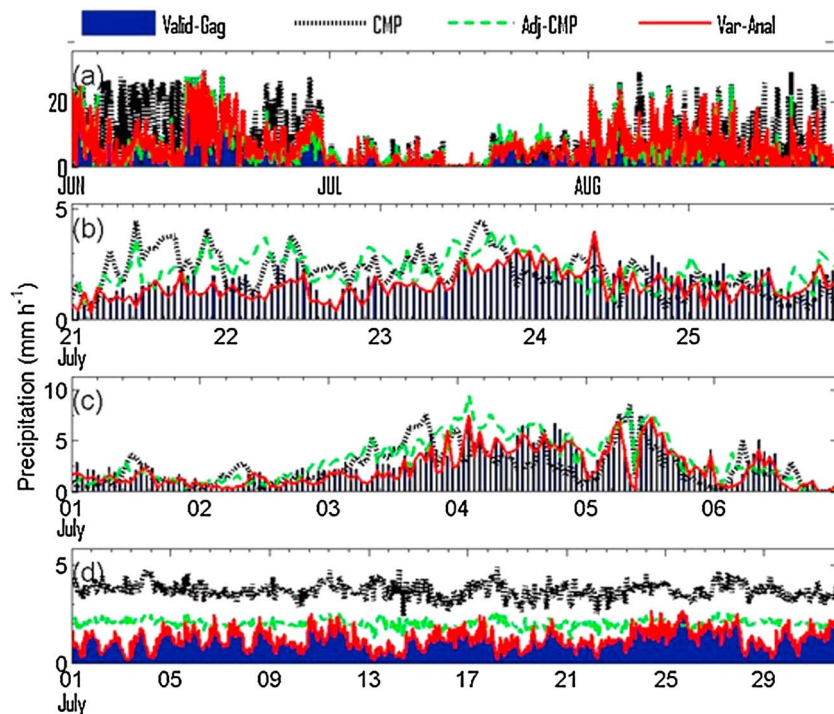


**Figure 11.** Time series of the hourly precipitation average from the validated data (gauge, black bar), original CMORPH (CMORPH, black dot line), bias-adjusted CMORPH (Adj-CMP, green dot line), and the rainfall analysis (var-anal, red solid line) over (a) the Yangtze River basin (28–33°N, 110–123°E), (b) south China region (21–24°N, 110–115°E), (c) southwest of Jiangsu Province (31–32°N, 118–119°E), and (d) data-sparse regions in Tibetan Plateau (25–40°N, 74–104°E).

comparison of the time series of precipitation for 1 June to 31 August 2009 shows that, especially in lower Yangtze River basin, the variational analysis performs best. It is found that variational analysis can well represent some precipitation structures near lower Yangtze River basins and Songhua River (Figure 11a). The time series of precipitation for two examples were shown in Figures 11b and 11c. Differences among those curves reflect the spatially averaged effects of spin-up/spin-down on the precipitation, while analysis nicely follows the gauge observations and satellite estimations, except analysis of the two others largely missed the strong precipitation around the Yangtze River and south China region. Cross-validation tests confirmed improved performance of the merged analysis in capturing spatial-temporal variations patterns as well as the PDF of the precipitation shown in Figure 12. The CMORPH products systematically underestimated rain rates compared to rain gauge, while the variational performs better into catching the temporal variations of rainfall. This indicates that the satellite estimated tends to underpredict the occurrence of heavy hourly rainfall. While the satellite estimates all the data sets largely missed the strong precipitation around the west regions, apparently due to their sparse gauge data in the area. The original CMORPH and adjusted CMORPH captured some precipitation structures Mainland of China systematically overestimated displayed over Tibetan high plateau in Figure 11d. The analysis is similar to the gauge observations, apparently due to their sparse gauge data in this area, such as Tibetan high plateau (Figure 11d), which show higher amounts but still clearly underestimate precipitation near in complex terrain. Over the Tibetan Plateau, the CMORPH simulations strongly overestimate the averaged precipitation by about 8.09% while the variational simulations reduce the bias to 0.34%.

Since rain gauge density is low to the north and west of the region, fine spatial-scale variability in precipitation extremes could be poorly revealed in this region. We examined how well the short-time heavy rainfall events are captured by our new merged products through comparison of the original CMORPH, the bias-adjusted CMORPH, and the variational analysis with independent gauge measurements. The impact of heavy rainfall occurrence integrate data for investigating short-time heavy rainfall occurrence compared to validation gauge observations (shown with black bar), original CMORPH (blue line), bias-adjusted CMORPH (green line) at 01–06 July 2009 in south China region and southwest of Jiangsu Province from 02:00 to 14:00 UTC,

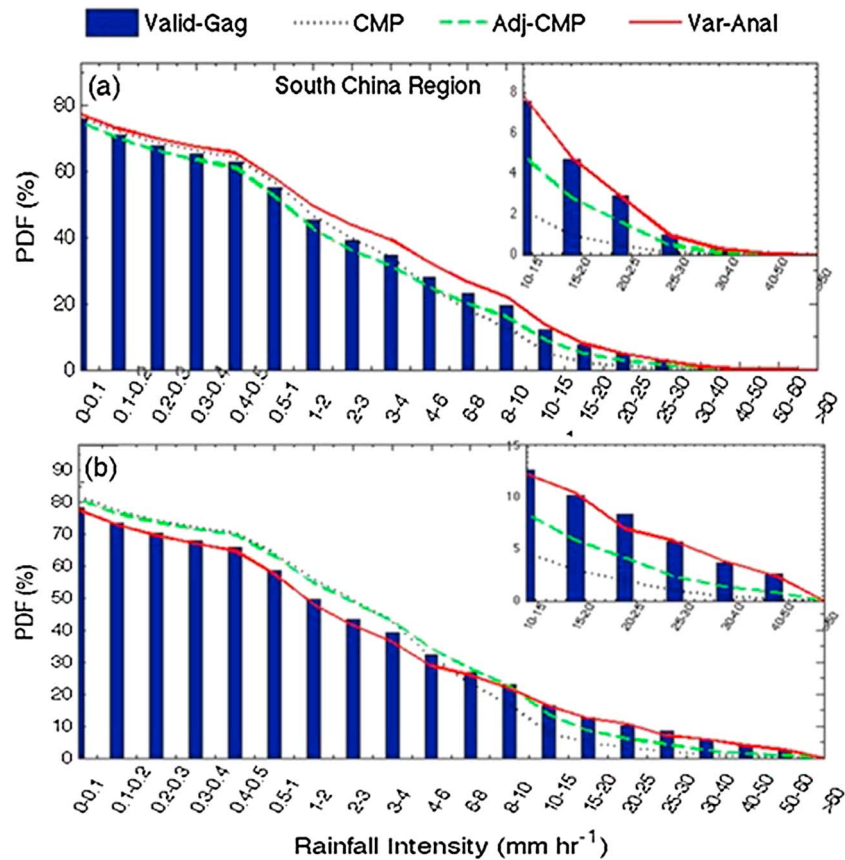


**Figure 12.** Probability density function (PDF, %) of hourly precipitation intensity at a 0.1° latitude/longitude grid box for the two examples impact of variational analysis for investigating short-time (hourly) heavy rainfall occurrences compared to validation gauge observations (shown with black bar), the original CMORPH (black dashed line), and biased adjusted CMORPH (green dot line) over (a) the south China region (21–24°N, 110–115°E) during 01–06 July 2009 and (b) the southwest of Jiangsu Province (31–32°N, 118–119°E) from 02:00 to 14:00 UTC, 07 July 2009. The plot in the top right for PDF from 10 to 60 mm h<sup>-1</sup> and more represent the dynamic range of the PDFs in heavy rainfall intensity.

07 July 2009. As shown in Figure 11, the heavy precipitation bands over rainfall occurrence were depicted very well in variational analysis with the maximum precipitation rate over 10 mm h<sup>-1</sup>. Figure 12 shows that the heavy precipitation bands over the south were depicted very well in analysis with the minimum bias -0.0430 mm h<sup>-1</sup>. It is also shown that the variational algorithm has no difficulty into integrating these extreme rain rates, which increases the correlation with the observation from 0.533 (CMORPH) to 0.790, reduces through the hourly mean bias by -0.09%. In the case of hourly precipitation, variational analysis has maxima greater than 8–9 mm h<sup>-1</sup> while rather few of satellite data exceeded this amount in study area. It means that there is poor agreement between the higher precipitation values: the mean maxima calculated from CMORPH are lower than the mean maxima calculate from the gridded data set. Perhaps it is not suspicious that satellite has been assumed to physically reach the saturation. This figure indicates that high-resolution at short-time integrating merged product is better to study for investigating short-time heavy rainfall events.

### 5. Conclusions and Future Work

A new variational technique for the analysis of hourly high-resolution precipitation has been presented, and the impact of merged data has been investigated with a case study of heavy rainfall over China. In the technique, a cost function is defined which measures the distance between analyzed precipitation field and observed precipitation quantity. The problem was then solved by minimizing the cost function that utilized a conjugate gradient method. The adjoint technique is used to drive the gradient of the cost function

with respect to analysis precipitation variable. At the minimum, the optimal estimate of precipitation is obtained. A recurve filter is used to spread observations to nearby grid points. The advantage of this technique is that all available information can be combined into an analysis according to their error sources in a simple flexible way.

Extensive evaluation of the original CMORPH, bias-adjusted CMORPH, and the variational analysis with the independent validated data confirmed the increasingly improved performance of the efforts. First of all, the bias in the original CMORPH precipitation has been adjusted substantially and the correlation for the bias-adjusted CMORPH is improved compared with that for the original CMORPH both at spatial domain and hourly time series comparison. The bias-adjusting approach is capable of removing the bias and increasing the pattern correlation consistently throughout the hourly evaluation period. The cross validation confirmed further improved the quality of the final combined hourly products that were further improved in capturing spatial-temporal variation patterns as well as the intensity of the precipitation at hourly time scales, particularly over the gauge network dense regions. The gauge-based analysis over the Tibetan high plain and western China is also refined in the combined analysis with the inclusion of information from the satellite estimates. A comparison among the gauge analysis, bias-adjusted CMORPH, and the analysis also indicates that differences between the gauge analysis and the analysis are relatively large over grid boxes with no gauges and decreases as local gauge network becomes dense. The differences between original satellite estimates and the analysis, meanwhile, are relatively large over regions with gauge stations. These results indicate that the combined analysis over gauge sparse regions is controlled primarily by satellite estimates while it is influenced more by gauge analysis where station reports are available, confirming that our objective algorithm works as we designed.

In addition, this paper suggests that the accurate detection and estimation of the type precipitation of light rainfall, solid precipitation, and orographic rainfall is still challenging for the future satellite precipitation retrievals. Aside from the temporal/spatial resolution issue, inaccuracies in situ measurements are especially impacted by wind effects at very short accumulation times under gauge catch which becomes worse as wind speed increases, especially for snow and light rain [Adam *et al.*, 2006]. Future advance in the detection of light and solid precipitation more reliably will make good use of assimilating Global Precipitation Measurement dual-frequency radar (K band) and the high-frequency channel of its radiometer. It is worth to apply Soil Moisture Active and Passive mission to evaluate the occurrence of light precipitation and compare rainfall forecast skill scores. The use of radar radial velocities would better capture dynamical structures especially in complex terrain.

#### Acknowledgments

This work is provided under the National Natural Science Foundation of China (41501471). The study is partially funded by Key Project of National Natural Science Foundation of China (91437214) and (71461010701). National Meteorological Information Center, CMA was acknowledged for giving access to their hourly rain gauge data (lih@igsnr.ac.cn), as well as appreciation is extended to Climate Prediction Center NOAA for providing CMORPH satellite estimates. The first author wishes to thank the computational facility supported by Hydrometeorology and Remote Sensing Laboratory and Advanced Radar Research Center at University of Oklahoma. Additionally, the first author also wishes to extend appreciation to the helpful suggestions of three reviewers.

#### References

- Adam, J. C., E. A. Clark, D. P. Lettenmaier, and E. F. Wood (2006), Correction of global precipitation products for orographic effects, *J. Clim.*, *19*, 15–38.
- Adler, R. F. (2003), The version-2 Global Precipitation Climatology Project (GPCP) monthly precipitation analysis (1979–present), *J. Hydrometeorol.*, *4*, 1147–1167.
- Arkin, P. A. (1979), The relationship between fractional coverage of high cloud and rainfall accumulations during GATE over the B-scale array, *Mon. Weather Rev.*, *107*, 1382–1387.
- Beck, C., J. Grieser, and B. Rudolf (2005), *A New Monthly Precipitation Climatology for the Global Land Areas for the Period From 1951 to 2000*, German Weather Service, Offenbach, Germany, Digital media.
- Boushaki, F.-I., K. L. Hsu, S. Sorooshian, and G.-H. Park (2009), Bias adjustment of satellite precipitation estimation using ground-based measurement: A case study evaluation over the southwestern United States, *J. Hydrometeorol.*, *10*, 1231–1242.
- Chen, M., W. Shi, P. Xie, V. B. Silver, V. E. Kousky, and J. E. Janowiak (2008), Assessing objective techniques for gauge-based analyses of global daily precipitation, *J. Geophys. Res.*, *113*, D04110, doi:10.1029/2007JD009132.
- Clarke R. (2010), A comparison of extreme rainfall characteristics in the Brazilian Amazon derived from two gridded data sets and a national rain gauge network, *J. Geophys. Res.*, *115*, D13104, doi:10.1029/2009JD013217.
- Courtier, P., E. Andersson, W. Heckley, D. Vasiljevic, M. Hamrud, A. Hollingsworth, F. Rabier, M. Fisher, and J. Pailleux (1998), The ECMWF implementation of three-dimensional variational assimilation (3D-Var). I: Formulation, *Q. J. R. Meteorol. Soc.*, *124*, 1783–1807.
- Dee, D. P. (2011), The ERA-Interim reanalysis: Configuration and performance of the data assimilation system, *Q. J. R. Meteorol. Soc.*, *137*, 553–597.
- Derb, J. (1987), Variational four-dimensional analysis using quasi-geostrophic constraints, *Mon. Weather Rev.*, *115*, 998–1008.
- Ebert, E. E., J. E. Janowiak, and C. Kidd (2007), Comparison of near-real-time precipitation estimates from satellite observations and numerical models, *Bull. Am. Meteorol. Soc.*, *88*, 47–64.
- Errico, R. M. (1997), What is an adjoint model?, *Bull. Am. Meteorol. Soc.*, *78*, 2577–2591.
- Ferraro, R. R. (1997), SSM/I derived global rainfall estimates for climatological applications, *J. Geophys. Res.*, *102*, 16,715–16,735, doi:10.1029/97JD01210.
- Gandin, L. S. (1965), Objective analysis of meteorological fields, *Israel Program for Scientific Translations*, 242 pp.
- Gao, J., M. Xue, K. Brewster, and K. K. Droegemeier (2004), A three-dimensional variational data analysis method with recursive filter for Doppler radars, *J. Atmos. Oceanic Technol.*, *21*, 457–469.

- Grill, P. E., W. Murray, and M. H. Wright (1981), *Practical Optimization*, 401 pp., Academic Press, New York.
- Habib, E., and G. J. Ciach (2001), Estimation of rainfall interstation correlation, *J. Hydrometeorol.*, *2*, 621–629.
- Hayden, C. M., and R. J. Purser (1995), Recursive filter objective analysis of meteorological fields: Applications to NESDIS operational processing, *J. Appl. Meteorol.*, *34*, 3–15.
- Hong, Y., K. L. Hsu, X. Gao, and S. Sorooshian (2004), Precipitation Estimation from Remotely Sensed Imagery using Artificial Neural Network-Cloud Classification System (PERSIANN-CCS), *J. Appl. Meteorol. Climatol.*, *43*(12), 1834–1853.
- Hong, Y., R. F. Adler, A. J. Negri, and G. J. Huffman (2007a), Flood and landslide applications of high-resolution satellite rainfall products, *J. Nat. Hazards*, *43*(2), 285–294, doi:10.1007/s11069-006-9106-x.
- Hong, Y., D. Gochis, J.-T. Cheng, K. L. Hsu, and S. Sorooshian (2007b), Evaluation of PERSIANN-CCS rainfall measurement using the NAME event rain gauge network, *J. Hydrometeorol.*, *8*, 469–482, doi:10.1175/JHM574.1.
- Hsu, K.-L., X. Gao, S. Sorooshian, and V. Gupta (1997), Precipitation Estimation from Remotely Sensed Information using Artificial Neural Networks, *J. Appl. Meteorol.*, *36*, 1176–1190.
- Huffman, G. J., R. F. Adler, B. Rudolf, U. Schneider, and P. R. Keehn (1995), Global precipitation estimates based on a technique for combining satellite-based estimates, rain gauge analysis, and NWP model precipitation information, *J. Clim.*, *8*, 1284–1295.
- Huffman, G. J., R. F. Adler, P. Arkin, A. Chang, R. Ferraro, A. Gruber, J. Janowiak, A. McNab, B. Rudolf, and U. Schneider (1997), The Global Precipitation Climatology Project (GPCP) version 1 data set, *Bull. Am. Meteorol. Soc.*, *78*, 5–20.
- Huffman, G. J., R. F. Adler, D. T. Bolvin, G. Gu, E. J. Nelkin, K. P. Bowman, E. F. Stocker, and D. B. Wolff (2007), The TRMM Multi-satellite Precipitation Analysis: Quasi-global, multi-year, combined-sensor precipitation estimates at fine scale, *J. Hydrometeorol.*, *8*, 38–55.
- Japan Meteorological Agency (JMA) Prediction Division (1990), Meteorological data and objective analysis, *Numerical Prediction Branch Tech. Rep.*, No. 36, pp. 109–131.
- Joyce, R. J., and P. Xie (2011), Kalman filter based CMORPH, *J. Hydrometeorol.*, *12*, 1547–1563, doi:10.1175/JHM-D-11-022.1.
- Joyce, R. J., J. E. Janowiak, P. A. Arkin, and P. Xie (2004), CMORPH: A method that produces global precipitation estimates from passive microwave and infrared data at high spatial and temporal resolution, *J. Hydrometeorol.*, *5*(3), 487–503.
- Kalnay, E. (2003), *Atmospheric Modeling, Data Assimilation and Predictability*, 341 pp., Cambridge Univ. Press, New York.
- Krajewski, W. F. (1987), Cokriging radar-rainfall and rain gauge data, *J. Geophys. Res.*, *92*(D8), 9571–9580, doi:10.1029/JD092iD08p09571.
- Krajewski, W. F., G. J. Ciach, and G. Villarini (2005), Towards probabilistic quantitative precipitation WSR-88D algorithms: Data analysis and development of ensemble generator model: Phase 4. Final Report to the Office of Hydrologic Development of the National Weather Service, Limited Distribution Rep., *IHR-Hydroscience & Engineering*, Univ. of Iowa, IA, 203 pp. [Available at [www.nws.noaa.gov/oh/hrl/papers/papers.htm#wsr88D](http://www.nws.noaa.gov/oh/hrl/papers/papers.htm#wsr88D).]
- Krajewski, W. F., et al. (2007), Towards better utilization of NEXRAD data in hydrology: An overview of Hydro-NEXRAD, Preprints, *World Environmental and Water Resources Congress 2007*, Tampa, FL, ASCE, 288–296. [Available at <http://cedb.asce.org/cgi/WWWdisplay.cgi?0705657>.]
- Kummerow, C., W. S. Olson, and L. Giglio (1996), A simplified scheme for obtaining precipitation and vertical hydrometeor profiles from passive microwave sensors, *IEEE Trans. Geosci. Remote Sens.*, *34*(5), 1213–1232.
- Kummerow, C., et al. (2001), The evolution of the Goddard Profiling Algorithm (GPROF) for rainfall estimation from passive microwave sensors, *J. Appl. Meteorol.*, *40*, 1801–1820.
- Lin, Y., and K. E. Mitchell (2005), The NCEP stage II/IV hourly precipitation analyses: Development and applications, *Preprints*, paper presented at 19th Conference on Hydrology, Am. Meteorol. Soc., San Diego, Calif.
- Liu, D. C., and J. Nosedal (1989), On the limited memory BFGS method for large scale optimization, *Math. Program.*, *45*, 503–528.
- Lopez, P. (2010), Direct 4D-Var assimilation of NCEP stage IV radar and gauge precipitation data at ECMWF, *Mon. Weather Rev.*, *139*, 2098–2116.
- Lopez, P., and P. Bauer (2005), “1D+4DVAR” assimilation of NCEP stage-IV radar and gauge hourly precipitation data at ECMWF, *Mon. Weather Rev.*, *135*, 2506–2524.
- Lorenc, A. C. (1981), A global three-dimensional multivariate statistical interpolation scheme, *Mon. Weather Rev.*, *109*, 701–721.
- Lorenc, A. C. (1992), Iterative analysis using covariance functions and filters, *Q. J. R. Meteorol. Soc.*, *118*, 569–591.
- Makihara, Y. (2000), Algorithms for precipitation nowcasting focused on detailed analysis using radar and raingauge data. in the “Study on the objective forecasting techniques”, *Tech. Rep. Meteorol. Res. Inst.*, *39*, 63–111.
- Morrissey, M. L., J. A. Maliekal, J. S. Greene, and J. Wang (1995), The uncertainty of simple averages using rain gauge networks, *Water Resour. Res.*, *31*, 2011–2017, doi:10.1029/95WR01232.
- New, M. G., M. Hulme, and P. D. Jones (2000), Representing twentieth century space-time climate variability. Part II: Development of a 1901–96 monthly grids of terrestrial climatology, *J. Clim.*, *13*, 2217–2238.
- Purser, R. J., and R. McQuigg (1982), A successive correction analysis scheme using recursive numerical filters, *Met. Office Tech. Note*, 154, British Meteor. Service, 17 pp.
- Purser, R. J., W.-S. Wu, D. F. Parrish, and N. M. Roberts (2003), Numerical aspects of the application of recursive filters to variational statistical analysis. Part I: Spatially homogeneous and isotropic Gaussian covariances, *Mon. Weather Rev.*, *131*, 1524–1535.
- Reynolds, R. W., and T. Smith (1994), Improved global sea surface temperature analyses using optimum interpolation, *J. Clim.*, *7*(6), 929–948.
- Rienecker, M. M., et al. (2011), MERRA: NASA’s Modern-Era Retrospective Analysis for Research and Applications, *J. Clim.*, *24*, 3624–3648, doi:10.1175/JCLI-D-11-00015.
- Rudolf, B. (1993), Management and analysis of precipitation data on a routine basis, in *Int. Symp. On Precipitation and Evaporation*, pp. 69–76, WMO, Bratislava, Slovakia.
- Saha, S., et al. (2010), The NCEP Climate Forecast System Reanalysis, *Bull. Am. Meteorol. Soc.*, *91*, 1015–1057, doi:10.1175/2010BAMS3001.1.
- Schneider, U. (1993), The GPCP quality-control system for gauge-measured precipitation data, *Proc. Analysis Methods for Precipitation on a Global Scale: Report of a GEWEX Workshop*, Koblenz, Germany, GPCP, WCRP-81, WMO/TD-588, A5-A9.
- Seo, D. J. (1999), Real-time estimation of rainfall fields using rain gauge data under fractional coverage conditions, *J. Hydrol.*, *223*, 131–147.
- Seo, D.-J., J. P. Breidenbach, R. A. Fulton, D. A. Miller, and T. O’Bannon (2000), Real-time adjustment of range-dependent bias in WSR-88D rainfall data due to nonuniform vertical profile of reflectivity, *J. Hydrometeorol.*, *1*, 222–240.
- Shen, Y., A.-Y. Xiong, Y. Wang, and P. Xie (2009), Performance of high-resolution satellite precipitation products over China, *J. Geophys. Res.*, *115*, D02114, doi:10.1029/2009JD012097.
- Sun, J., and N. A. Crook (2001), Real-time low-level wind and temperature analysis using single WSR-88D data, *Weather Forecasting*, *16*, 117–132.
- Talagrand, O., and P. Courtier (1987), Variational Assimilation of Meteorological Observations with the Adjoint Vorticity Equation. Part I: Theory, *Q. J. R. Meteorol. Soc.*, *113*, 1311–1328.
- Thiébaux, J., E. Rogers, W. Wang, and B. Katz (2003), A new high-resolution blended real-time global sea surface temperature analysis, *Bull. Am. Meteorol. Soc.*, *84*, 643–656.

- Tian, Y., C. D. Peters-Lidard, B. J. Choudhury, and M. Garcia (2007), Multitemporal analysis of TRMM-based satellite precipitation products for land data assimilation applications, *J. Hydrometeorol.*, *8*, 1165–1183, doi:10.1175/2007JHM859.1.
- Tian, Y., C. D. Peters-Lidard, J. B. Eylander, R. J. Joyce, G. J. Huffman, R. F. Adler, K.-L. Hus, F. J. Turk, M. Garcia, and J. Zeng (2009), Component analysis of errors in satellite-based precipitation estimates, *J. Geophys. Res.*, *114*, D24101, doi:10.1029/2009JD011949.
- Turk, F. J., E. E. Ebert, B.-J. Sohn, H.-J. Oh, V. Levizzani, E. A. Smith, and R. Ferraro (2004), Validation of an operational global precipitation analysis at short time scales, *12th AMS Conf. on Satellite Meteorology and Oceanography*, Seattle, Wash., 11–15 Jan.
- Ushio, T., et al. (2009), A Kalman filter approach to the Global Satellite Mapping of Precipitation (GSMaP) from combined passive microwave and infrared radiometric data, *J. Meteorol. Soc. Jpn.*, *87A*, 137–151.
- Vasiloff, S. V., et al. (2007), Improving QPE and very short term QPF, *Bull. Am. Meteorol. Soc.*, *88*, 1899–1911, doi:10.1175/BAMS-88-12-1899.
- Villarini, G., and W. F. Krajewski (2008), Empirically-based modelling of spatial sampling uncertainties associated with rainfall measurement by rain gauges, *Adv. Water Resour.*, *31*, 1015–1023.
- Villarini, G., P. V. Mandapaka, W. F. Krajewski, and R. J. Moore (2008), Rainfall and sampling uncertainties: A rain gauge perspective, *J. Geophys. Res.*, *113*, D11102, doi:10.1029/2007JD009214.
- Wang, W., and P. Xie (2006), A multiplatform-merged (MPM) SST analysis, *J. Clim.*, *20*, 1662–1679.
- Wang, W., P. Xie, S.-H. Yoo, Y. Xue, A. Kumar, and X. Wu (2011), An assessment of the surface climate in the NCEP Climate Forecast System Reanalysis, *Clim. Dyn.*, *37*, 1601–1620.
- Xie, P., and P. A. Arkin (1996), Analyses of global monthly precipitation using gauge observations, satellite estimates, and numerical model predictions, *J. Clim.*, *9*, 840–858.
- Xie, P., and P. A. Arkin (1997), Global precipitation: A 17-year monthly analysis based on gauge observations, satellite estimates and numerical model outputs, *Bull. Am. Meteorol. Soc.*, *78*, 2539–2558.
- Xie, P., and Y. Hong (2011), Integrating information from multiple sources for improved precipitation products, *AGU Hydrology Section News Letter*, May.
- Xie, P., and A. Y. Xiong (2011), A conceptual model for constructing high-resolution gauge-satellite merged precipitation analyses, *J. Geophys. Res.*, *116*, D21106, doi:10.1029/2011JD016118.
- Xie, P., J. E. Janowiak, P. A. Arkin, R. F. Adler, A. Gruber, R. Ferraro, G. J. Huffman, and S. Curtis (2003), GPCP pentad precipitation analyses: An experimental dataset based on gauge observations and satellite estimates, *J. Clim.*, *16*, 2197–2214.
- Xie, P., M. Chen, A. Yatagai, T. Hayasaka, Y. Fukushima, and S. Yang (2007), A gauge-based analysis of daily precipitation over East Asia, *J. Hydrometeorol.*, *8*, 607–626.
- Xie, P., T. Boyer, E. Bayler, Y. Xue, D. Byrne, J. Reagan, R. Locarnini, and A. Kumar (2012), NOAA blended analysis of surface salinity: Preliminary results, *7th Aquarius/SAC-D Science Meeting*, 11–13 April 2012, Buenos Aires, Argentina.
- Yoo, S.-H., P. Xie, and W. Wang (2011), Global precipitation diurnal variations depicted in the observation and the CFS Reanalysis, *91th AMS Annual Meeting*, Seattle, Wash., 23–27 Jan.
- Zhang, J., et al. (2011), National Mosaic and Multi-sensor QPE(NMQ) System description, results, and future plans, *Bull. Am. Meteorol. Soc.*, *92*, 1321–1331, doi:10.1175/2011BAMS-D-11-00047.1.